J. Phys. G: Nucl. Phys. **10** (1984) 1683–1701. Printed in Great Britain

Systematics of nuclear RMS charge radii

B A Brown†, C R Bronk‡ and P E Hodgson‡

† Cyclotron Laboratory, Michigan State University, East Lansing, Michigan 48824, USA
‡ Nuclear Physics Laboratory, University of Oxford, Keble Road, Oxford OX1 3RH, UK

Received 4 June 1984

Abstract. The experimental RMS charge radii of isotopic sequences of nuclei are compared with calculations based on the spherical droplet model and spherical single-particle potential models. Harmonic-oscillator, Woods–Saxon and Skyrme Hartree–Fock single-particle potentials are considered. Deviations between experiment and theory are discussed in terms of the model parameters and in terms of the fundamental inadequacies of the models. The experimental B(E2) values connecting the ground states and the lowest 2^+ states are used to estimate the increase in RMS radius due to the effects of deformation and zero-point vibrational motion.

1. Introduction

One of the most fundamental properties of a nucleus which must be understood and reproduced by nuclear models is its spatial extension. The most easily obtainable and usually most accurate measure of the spatial extent which can be determined experimentally is the root-mean-square (RMS) charge radius as determined by electromagnetic probes. For stable nuclei these RMS radii can be obtained from electron elastic scattering cross sections and from the x-ray transition energies of muonic atoms (Barrett and Jackson 1977). In addition, the relative RMS radii of a series of isotopes can be extracted from the isotope shifts of atomic x-ray transitions. With the improved laser-spectrographic techniques of measuring x-ray transitions in atomic beams, it has become possible to study unstable nuclei produced in nuclear reactions with half-lives of the order of microseconds or greater. Within the last few years many long chains of such isotopes have been studied in this way (see, e.g., the references given in table 1 for the Na, K, Ca, Kr, Rb, Cd, Cs, Ba, Sm, Hg and Pb isotopes).

The purpose of the present paper is to compare in a systematic way essentially all available experimental RMS charge radii with the predictions of a number of phenomenological prescriptions and theoretical models. Theoretical background for our calculations is provided by the extensive works of Sorensen and his collaborators (Uher and Sorensen 1966, Sorensen 1966, Reehal and Sorensen 1971). They introduce the ideas of monopole and quadrupole core-polarisation corrections to the spherical liquid-drop model. We extend their calculations by making use of the 'droplet' model (Myers 1977, 1982, Myers and Schmidt 1983) in place of the liquid-drop model. The monopole core polarisation is taken into account in our calculations by considering the spherical single-particle potentials based on the harmonic-oscillator, Woods–Saxon and Skyrme Hartree–Fock models. For the quadrupole core polarisation we consider the empirical corrections based on the properties of the lowest 2^+ states. The recent extensions of

0305-4616/84/121683 + 19$02.25

Esbensen and Bertsch (1983) for the higher multipole core-polarisation effects are discussed briefly. This study is limited to comparisons using potential parameters which have been proposed previously, and we have not attempted to adjust the parameters to achieve optimal agreement with experiment. Our comparisons should provide background and motivation for further theoretical developments.

The data considered are summarised in table 1. We have started from the 1974 compilations of de Jager *et al*, Engfer *et al*, Boehm and Lee, and Heilig and Steudel. These have then been supplemented with more recent data. We have chosen the most recent and most comprehensive experimental results reported, and no attempt has been made to provide an average with earlier results other than those provided in the references cited. Some discrepancies have been noted in the footnotes to table 1. Two columns of references are given in table 1. The first lists the reference for the relative isotope shift measurements. The second column of references refers to the absolute RMS radius of one of the stable nuclei in each isotopic chain whose value is given in the table. In a few cases the absolute radius has not been measured or has not been determined accurately enough to be meaningful in the present comparison. In these cases we have arbitrarily chosen a value for the absolute radius for one of the stable isotopes. In the figures discussed below, these 'floating' isotopic chains are distinguished by special symbols. The models we will compare with are appropriate for 'many-nucleon' systems, and we will consider comparisons only for $Z > 7$.

It is well known that the RMS radii scale roughly as $A^{1/3}$. By analogy with the properties of an incompressible fluid this fact leads to the nuclear liquid-drop (LD) model. In its simplest form the nucleus is considered to have a sharp surface with radius $R_0 = r_0 A^{1/3}$ and the RMS radius is given by

$$\text{RMS(LD}, A) = (\tfrac{3}{5})^{1/2} r_0 A^{1/3}. \tag{1}$$

Table 1. RMS radii: references and normalisations.

Isotope		Relative radii Reference	Absolute normalisation		
			N	RMS(fm)	Reference
0	n		1	[a]	Chandra and Sauer (1976)
1	H		0	0.88	Chandra and Sauer (1976)
2	He	McCarthy *et al* (1977)	2	1.671(22)	Sick *et al* (1976)
3	Li	Suelzle *et al* (1967)	3	2.51(10)	Bumiller *et al* (1972)
4	Be		5	2.519(12)	de Jager *et al* (1974)
5	B	Olin *et al* (1981)	5	2.44(6)	Olin *et al* (1981)
6	C	Schaller *et al* (1982)	6	2.472(16)	Schaller *et al* (1982)
7	N	Schutz (1975)	7	2.540(20)	Schutz (1975)
8	O	Miska *et al* (1979)	8	2.710(15)	Kim *et al* (1978)
9	F		8	2.898(10)[b]	Schaller *et al* (1978)
10	Ne	Singhal *et al* (1975)	8	3.020(20)	de Jager *et al* (1974)
11	Na[c]	Huber *et al* (1978)	12	2.986(9)	Schaller *et al* (1978)
12	Mg	Euteneuer *et al* (1977) de Jager *et al* (1974)	12	3.035(18)	Li *et al* (1974)
13	Al		14	3.058(5)[b]	Schaller *et al* (1978)
14	Si	Engfer *et al* (1974)	14	3.125(5)[d]	Schaller *et al* (1978)
15	P		14	3.187(3)[b]	Schaller *et al* (1978)
16	S	Rychel *et al* (1983)	16	3.263(2)[d]	Schaller *et al* (1978)
17	Cl	Briscoe *et al* (1980)	17	3.388(15)[b]	Briscoe *et al* (1980)
18	Ar	Fricke *et al* (1982)	18	3.396(7)[e]	Daniel *et al* (1974)
19	K[f]	Touchard *et al* (1982)	20	3.436(3)[d]	Schaller *et al* (1982)
20	Ca	Andl *et al* (1982)	20	3.481(5)[g]	Wohlfahrt *et al* (1981)

Table 1. (continued)

Isotope		Relative radii Reference	Absolute normalisation		
			N	RMS(fm)	Reference
21	Sc	Wohlfahrt *et al* (1981)	24	3.550(5)[b, g]	Wohlfahrt *et al* (1981)
22	Ti	Wohlfahrt *et al* (1981)	28	3.574(5)[g]	Wohlfahrt *et al* (1981)
23	V	Wohlfahrt *et al* (1981)	28	3.603(5)[b, g]	Wohlfahrt *et al* (1981)
24	Cr[h]	Wohlfahrt *et al* (1981)	28	3.645(5)[g]	Wohlfahrt *et al* (1981)
25	Mn	Wohlfahrt *et al* (1981)	30	3.710(5)[b, g]	Wohlfahrt *et al* (1981)
26	Fe	Wohlfahrt *et al* (1980)	28	3.694(5)[g]	Wohlfahrt *et al* (1980)
27	Co		32	3.793(5)[b, i]	Shera *et al* (1976)
28	Ni	Wohlfahrt *et al* (1980)	30	3.777(5)[i]	Shera *et al* (1976)
29	Cu	Shera *et al* (1976)	34	3.888(5)[i]	Shera *et al* (1976)
30	Zn	Wohlfahrt *et al* (1980)	34	3.932(5)	Wohlfahrt *et al* (1980)
31	Ga				
32	Ge[j]	Kline *et al* (1975)	38	4.07(2)[j]	Kline *et al* (1975)
33	As				
34	Se				
35	Br				
36	Kr	Gerhardt *et al* (1979)	50	4.160	Arbitrary
37	Rb	Thibault *et al* (1981a)	50	4.180	Arbitrary
38	Sr[k]	Heilig and Steudel (1974)			
39	Y		50	4.239(7)[b]	Engfer *et al* (1974)
40	Zr	Rothhaas (1976)	50	4.263(8)	Rothhaas (1976)
41	Nb		52	4.318(3)[b]	Engfer *et al* (1974)
42	Mo	Schellenberg *et al* (1980)	50	4.317(4)	Schellenberg *et al* (1980)
43	Tc				
44	Ru[k]	Heilig and Steudel (1974)			
45	Rh		58	4.51(4)	Engfer *et al* (1974)
46	Pd[k]	Heilig and Steudel (1974)	64	4.595(3)	Lightbody *et al* (1976)
47	Ag				
48	Cd	Heilig and Steudel (1974) Wenz *et al* (1981)[l]	62	4.578(7)	Gillespie *et al* (1975)
49	In		66	4.619(15)[b]	Engfer *et al* (1974)
50	Sn	Heilig and Steudel (1974)	66	4.623(1)[m]	Cavedon (1980)
51	Sb	Boehm and Lee (1974)	70–72	4.676(5)[b]	Engfer *et al* (1974)
52	Te	Boehm and Lee (1974)	74	4.774(6)	Engfer *et al* (1974)
53	I		74	4.763(6)[b, n]	Engfer *et al* (1974)
54	Xe	Boehm and Lee (1974)	82	4.784	Arbitrary
55	Cs	Thibault *et al* (1981b)[o]	78	4.800(7)[n]	Engfer *et al* (1974)
56	Ba	Bekk *et al* (1979) Shera *et al* (1982)	82	4.832(1)	Shera *et al* (1982)
57	La[b, k]	Heilig and Steudel (1974)	82	4.861(8)[b, n]	Engfer *et al* (1974)
58	Ce[b]	Heilig and Steudel (1974)	82	4.883(9)[b, n]	Engfer *et al* (1974)
59	Pr		82	4.881(9)[b, n]	Engfer *et al* (1974)
60	Nd	Heilig and Steudel (1974)	82	4.913(10)[n]	Engfer *et al* (1974)
61	Pm				
62	Sm	Heilig and Steudel (1974)	86	5.002(6)	Moinester *et al* (1981)
63	Eu[b]	Heilig and Steudel (1974)	90	5.104[b]	Arbitrary
64	Gd	Heilig and Steudel (1974) Laubacher *et al* (1983)	92	5.141(3)	Laubacher *et al* (1983)
65	Tb				
66	Dy	Neugart (1982)[p]	92	5.181	Arbitrary
67	Ho				
68	Er	Neugart (1982)[p]	92	5.220	Arbitrary
69	Tm				
70	Yb	Neugart (1982)[p]	92	5.260	Arbitrary

Table 1. (continued)

Isotope		Relative radii Reference	Absolute normalisation		
			N	RMS(fm)	Reference
71	Lu				
72	Hf	Heilig and Steudel (1974)	104	5.350	Arbitrary
73	Ta				
74	W[k]	Heilig and Steudel (1974)			
75	Re[k]	Heilig and Steudel (1974)			
76	Os	Heilig and Steudel (1974)	114	5.389	Arbitrary
77	Ir				
78	Pt[k]	Heilig and Steudel (1974)			
79	Au	Kluge *et al* (1983)	118	5.434(2)	Engfer *et al* (1974)
80	Hg	Bonn *et al* (1976)[q]	124	5.496	Arbitrary
81	Tl[k]	Heilig and Steudel (1974) Engfer *et al* (1974)	124	5.484(6)	Engfer *et al* (1974)
82	Pb	Thompson *et al* (1983)	126	5.503(2)	Cavedon (1980)
83	Bi[k]	Heilig and Steudel (1974)	126	5.521(2)	de Jager *et al* (1974)
84	Po				
85	At				
86	Rn				
87	Fr				
88	Ra				
89	Ac				
90	Th[k]	Heilig and Steudel (1974)	142	5.773	de Jager *et al* (1974)
91	Pa				
92	U[k]	Heilig and Steudel (1974)	146	5.843	de Jager *et al* (1974)
93	Np				
94	Pu	Heilig and Steudel (1974)	144	5.860	Arbitrary
95	Am[k]	Heilig and Steudel (1974)			
96	Cm[k]	Heilig and Steudel (1974)			

[a] The mean-square charge radius for the neutron is -0.116 fm^2.

[b] These data were not included in the figures since there were only a few points in the isotopic chain which tended to overlap those of longer neighbouring chains.

[c] We note in this case that the systematic errors due to uncertainties in the 'mass shift' are rather large for nuclei far from the stability line (Huber *et al* 1978).

[d] Corrections for the small isotopic abundances of other naturally occurring isotopes have been made.

[e] The ^{36}Ar radius given by Daniel *et al* (1974) does not agree with Finn *et al* (1976), perhaps because only the statistical errors are quoted in the latter work.

[f] We note in this case that the systematic errors due to uncertainties in the 'mass shift' are rather large for nuclei far from the stability line (Touchard *et al* 1982).

[g] The values are taken from table VI of Wohlfahrt *et al* (1981) and the errors are based on the typical errors given in table V of Wohlfahrt *et al* (1980).

[h] The RMS radii given by Wohlfahrt *et al* for Cr isotopes are consistent with the work reported recently by Lightbody *et al* (1976, 1983).

[i] The values are taken from table VII of Shera *et al* (1976) and the errors are based on the typical errors given in table V of Wohlfahrt *et al* (1980).

[j] Not used in the figures because of the relatively large error.

[k] Only relative isotope shifts are given by Heilig and Steudel (1974) in this case and are thus not included in our analysis.

[l] The isotopes shifts given by Wenz *et al* (1981) are consistent with those of van Eijk *et al* (1979).

[m] This value is somewhat inconsistent with the value of 4.642(6) fm given by Lightbody *et al* (1976).

[n] We do not include the systematic error seen in the two different analyses of ^{127}I given by Engfer *et al* (1974).

[o] These results are consistent with those of Schinzler *et al* (1978).

[p] Taken from figure 7 of the paper by Neugart (1982).

[q] The change in mean-square radii was taken from the λ (exp) column in table 3 of Bonn *et al* (1976).

In figure 1 the experimental radii are compared with equation (1) using the value of $r_0 = 1.2$ fm which optimises the agreement for large values of A. The experimental RMS radii for smaller A are systematically larger than the liquid-drop-model prediction. This can be understood as being due to the surface diffuseness. Myers and Schmidt (1983) have taken the diffuseness into account in the 'extended-liquid-drop' model by folding the sharp-surface charge distribution with a normalised, spherically symmetric, short-ranged function. They used a gaussian function, $\exp(-r^2/2b^2)$, with a value of $b = 0.99$ fm obtained from a best fit to experiment. The parameter b is assumed to be independent of N and Z. The RMS radii in this extended-liquid-drop (ELD) model are given by (Myers and Schmidt 1983)

$$\text{RMS(ELD}, A) = (\tfrac{3}{5})^{1/2}(1.15 + 1.80A^{-2/3} - 1.20A^{-4/3})A^{1/3} \text{ fm}. \tag{2}$$

In figure 1 the experimental radii are compared with equation (2). The qualitative agreement is now much better for the lighter nuclei, but on a more quantitative level there are significant deviations relative to the ELD model. In order to emphasise these deviations, in figure 2(*a*) we plot the difference RMS(expt) − RMS(ELD). In the remainder of this paper, we will study the possible origins of these deviations with the help of more refined theoretical models. Graphical comparisons of experiment and theory are shown in figures 2 and 3.

In figures 2(*a*)–(*e*) the differences between experimental and theoretical RMS charge radii are plotted. The points representing nuclei of a given isotopic chain are connected by lines. The symbols at the beginning and end of each line indicate those with an even value

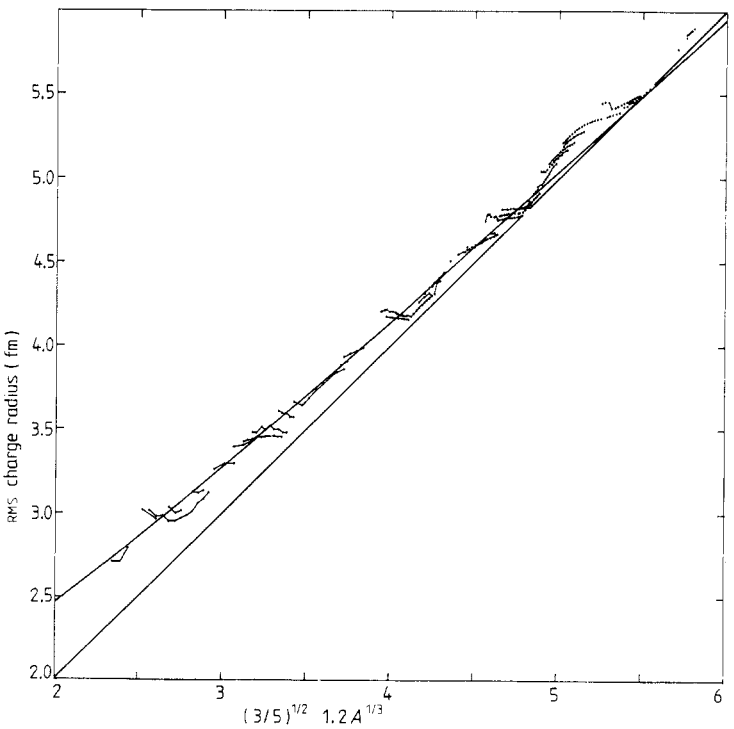

Figure 1. Plot of the experimental RMS charge radii on the y axis as a function of $(\frac{3}{5})^{1/2}\,1.2\,A^{1/3}$ on the x axis. On the y axis we also compare the calculation with the extended-liquid-drop model using equation (2).

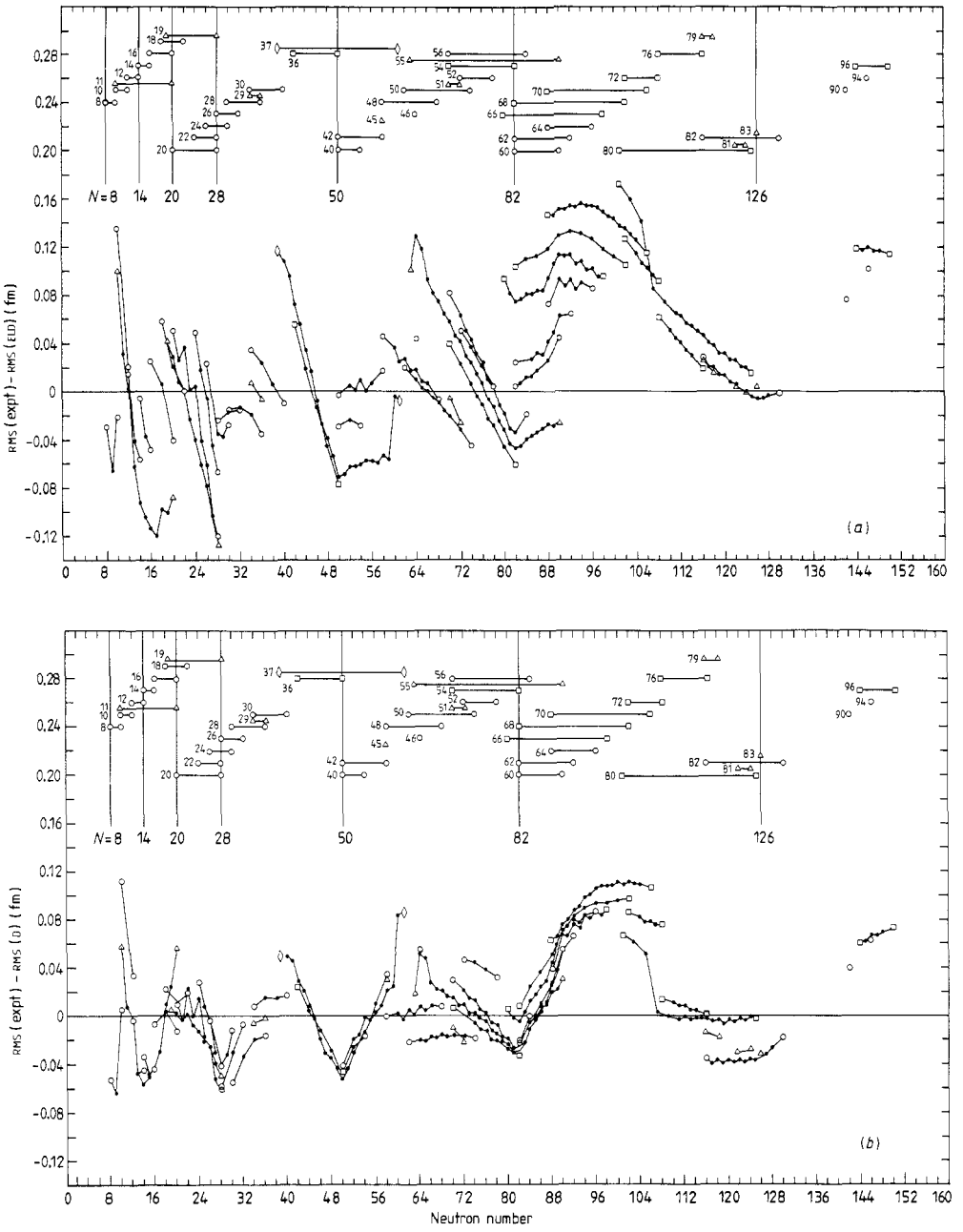

Figure 2. Differences between experiment and theoretical RMS charge radii. The comparison is made for (*a*) the extended-liquid-drop model (ELD), (*b*) the droplet model (D), (*c*) the harmonic-oscillator potential model (HO), (*d*) the Woods–Saxon potential model (WS), (*e*) the Skyrme-3 Hartree–Fock potential model (SK3) and (*f*) the SGII Hartree–Fock potential model (SGII). Isotopic chains are connected by lines with special symbols at the ends. We use circles for the even-Z isotopes with experimental absolute normalisation, squares for the even-Z isotopes with arbitrary normalisation, triangles for the odd-Z isotopes with experimental absolute normalisation and diamonds for the odd-Z isotopes with arbitrary normalisation.

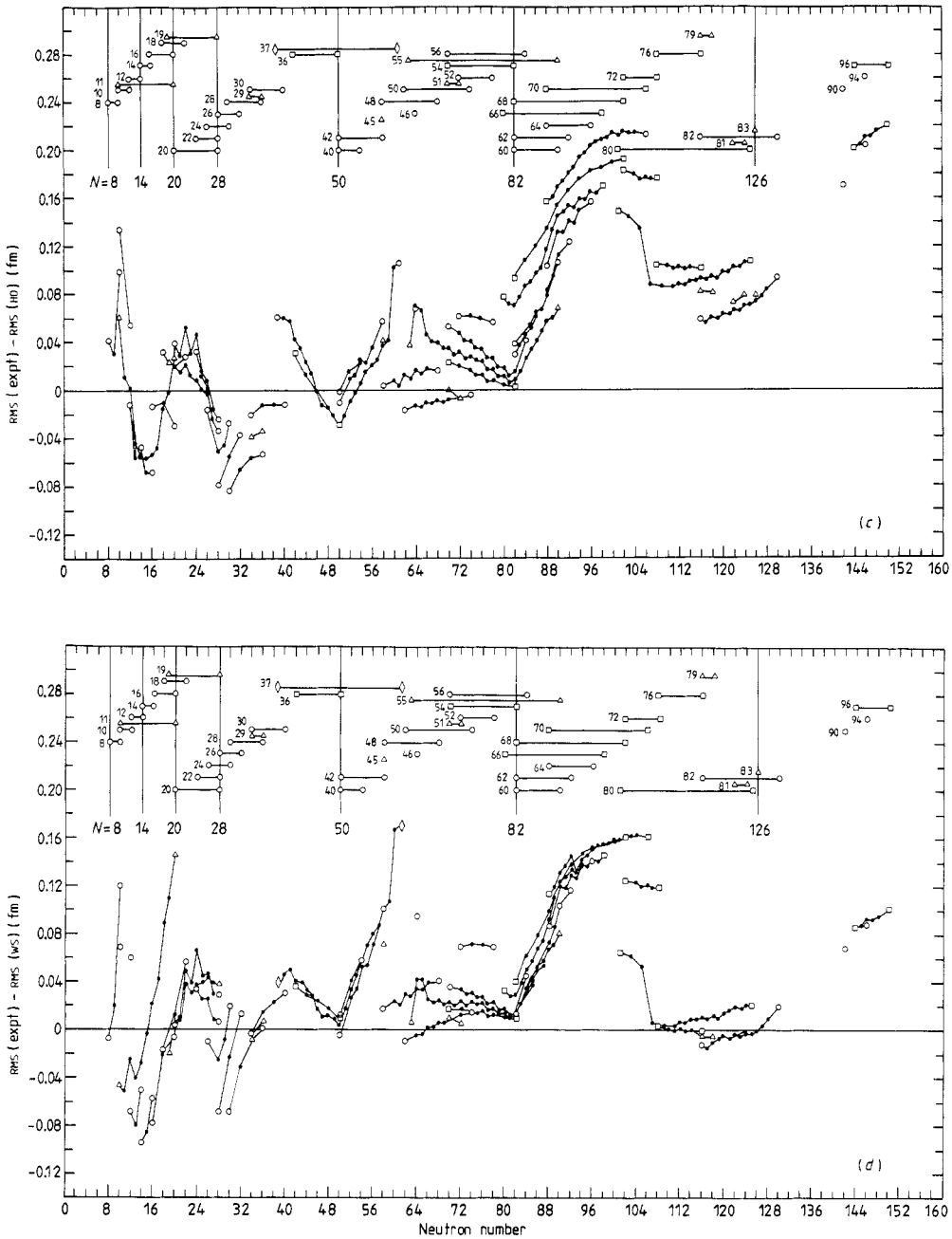

Figure 2. (continued)

of Z (circles and squares) and those with an odd value of Z (triangles and diamonds). The isotopes for which an experimental value was used for the absolute radius are indicated by the circles and triangles and the 'floating' isotopic chains are indicated by the squares and diamonds. The particular value of Z of each chain can be inferred from the labels at the top

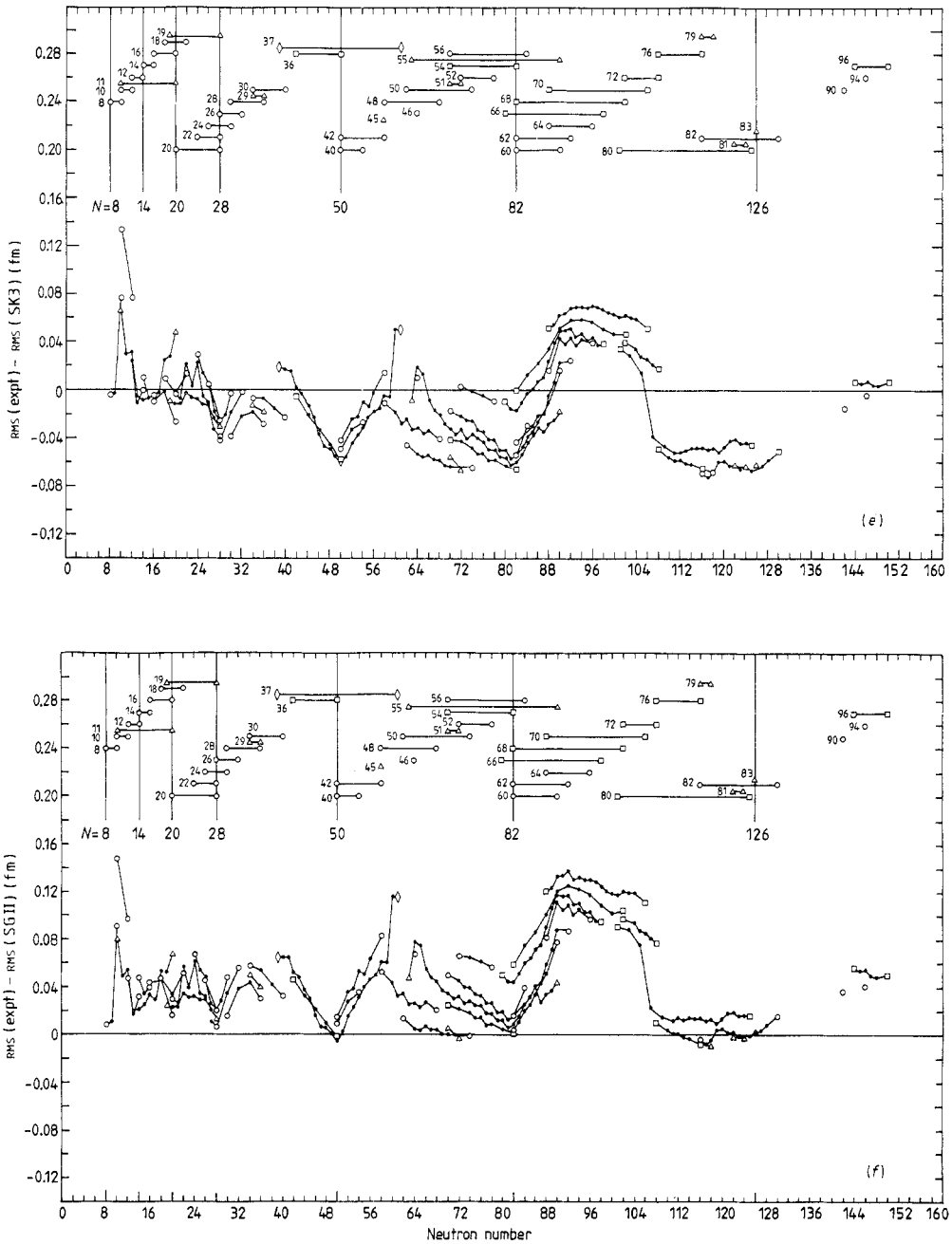

Figure 2. (continued)

of the figures which are placed directly above the data. For clarity, experimental error bars have not been included in the figures. The absolute errors are given in table 1 and the relative errors are given in the references cited there. In general the errors are small compared with the deviations between experiment and theory.

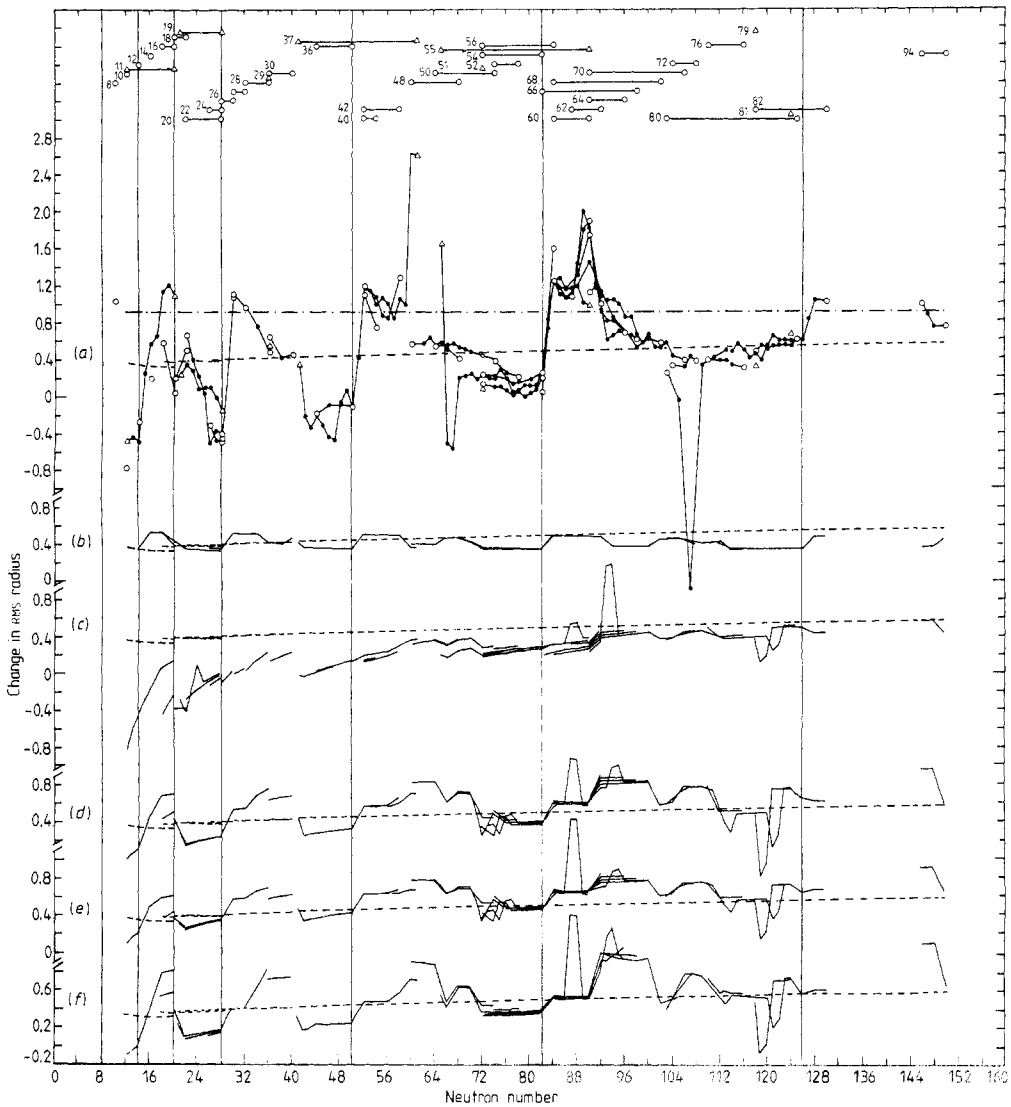

Figure 3. Brix–Kopfermann plot for the isotope shift relative to that of the liquid-drop model (see equation (3)). In (*a*) the experimental relative isotope shift is compared with the results of the calculations based on the extended-liquid-drop model (chain line) and the droplet model (broken line). For the experiment, isotopes with even (odd) Z are indicated by circles (triangles) at the beginning and end of the lines. In (*b*)–(*e*) the droplet-model predictions are compared with the results of the calculations based on single-particle potentials; (*b*) the harmonic-oscillator potential (HO); (*c*) the Woods–Saxon potential (WS); (*d*) the Skyrme-3 Hartree–Fock potential (SK3); (*f*) the SGII Hartree–Fock potential (SGII). The calculation shown in (*e*) is the same as that of (*d*) except that the neutron finite-size and relativistic spin–orbit contributions to the charge density are excluded.

Since the relative RMS radii within a given isotopic chain are sometimes known more accurately than the absolute radii, it is useful to present the comparisons for the isotope shifts in the form of a Brix–Kopfermann (Brix and Kopfermann 1958) plot. The quantities in the BK plot are the differences in the mean-square ($\text{MS} = \text{RMS}^2$) charge radii between

isotopes differing by two neutrons divided by the differences expected from the liquid-drop (LD) model:

$$\text{BK}(\text{expt}, Z, N) = \frac{\text{MS}(\text{expt}, Z, N) - \text{MS}(\text{expt}, Z, N-2)}{\text{MS}(\text{LD}, A) - \text{MS}(\text{LD}, A-2)}. \tag{3}$$

The quantities BK(expt), which we will refer to hereafter as the relative isotope shifts, are plotted in figure 3(*a*). The experimental points representing nuclei within a given isotopic chain are connected by lines. The symbols at the beginning and end of each line indicate those with an even value of Z (circles) and those with an odd value of Z (triangles). The particular value of Z for each chain can be inferred from the labels at the top of the figures which are placed directly above the data. An earlier comparison of the data in this form is given in figure 2 of the compilation of Heilig and Steudel (1974). In figures 3(*a*)–(*f*) model predictions obtained by using equation (3) with theoretical values in place of experimental ones are shown.

In the following sections we will describe the models which we have used to calculate the RMS charge radii and discuss the comparison between experiment and theory. In § 2 the droplet model of Myers (1977) and Myers and Schmidt (1983) is discussed. (Note that we use the terms liquid drop, extended liquid drop and droplet to refer to three distinct models.) The spherical single-particle potential models are described in § 3. In § 4 we discuss the comparison between theory and experiment and consider the additional contributions to the theoretical radii due to the effects of deformation and zero-point vibrational motion.

2. The droplet model

In figure 3(*a*) the experimental relative isotope shifts are compared with the predictions of the extended-liquid-drop (equation (2)) model given by the chain line. There are large fluctuations, but on average the experimental relative isotope shift is about half of that expected from the ELD model. Conversely, it follows that the isotone shift must on average be greater than that of the ELD model in order that the radii be proportional on average to $A^{1/3}$.

This inadequacy of the ELD model has been overcome in the 'droplet' model of Myers by allowing for a neutron skin. We present here a summary of the spherical droplet-model equations which were obtained by Myers and Schmidt (1983) by minimising the macroscopic energy of the droplet. The sharp-surface radius R_m for the matter density (the sum of neutrons and protons) is given by

$$R_m = r_0 A^{1/3}(1 + \bar{\varepsilon}) \tag{4}$$

where

$$\bar{\varepsilon} = (-2a_2 A^{-1/3} + L\bar{\delta}^2 + c_1 Z^2 A^{-4/3})/K \tag{5}$$

$$\bar{\delta} = \frac{(N-Z)/A + \frac{3}{16}(c_1/Q)ZA^{-2/3}}{1 + \frac{9}{4}(J/Q)A^{-1/3}} \tag{6}$$

and

$$c_1 = \tfrac{3}{5}e^2/r_0. \tag{7}$$

The parameters have been obtained by a fit to nuclear binding energies and radii (Myers 1977): $r_0 = 1.18$ fm (the nuclear radius constant), $a_2 = 20.69$ MeV (the surface energy constant), $J = 36.8$ MeV (the symmetry energy constant), $Q = 17$ MeV (the effective surface stiffness), $K = 240$ MeV (the incompressibility coefficient) and $L = 100$ MeV (the density symmetry energy).

The proton and neutron sharp-surface radii are then given by

$$\begin{aligned} R_p &= R_m - (Z/A)t \\ R_n &= R_m + (N/A)t \end{aligned} \tag{8}$$

where t is the neutron skin thickness given by

$$t = \tfrac{2}{3}R_m\{[(N-Z)/A] - \bar{\delta}\}. \tag{9}$$

Including diffuseness and 'redistribution' corrections, the RMS charge radius for the protons in the spherical droplet model (D) is given by

$$\text{RMS(D}, Z, N) = [3b^2 + \tfrac{3}{5}(R_p^2 + R_r^2)]^{1/2}. \tag{10}$$

The first term on the left-hand side arises from folding the gaussian diffuseness described above in connection with the ELD model. The contribution from R_r is the 'redistribution' term which results from a more exact treatment of the Coulomb potential

$$R_r^2 = \tfrac{4}{35}C'R_p^2 \tag{11}$$

where

$$C' = \tfrac{1}{2}[(9/2K) + (1/4J)]Ze^2/R_p. \tag{12}$$

The differences RMS(expt) − RMS(D) are shown in figure 2(*b*) and the relative isotope shift is shown in figure 3(*a*) (broken line). The average isotope shift obtained in the droplet model is about half that obtained from the liquid-drop and ELD models and is in better agreement with the experimental average. The relative isotope shift is predicted to increase slightly with A from about 0.3 for $A = 16$ to 0.55 for $A = 208$. This is difficult to verify experimentally because of the large experimental flucations about the average. The values of RMS(expt) − RMS(D) (figure 2(*b*)) show much more clustering than was obtained in the RMS(expt) − RMS(ELD) comparison (figure 2(*a*)), indicating that the isotone shift is also better described in the droplet model.

The deviations in $\Delta R = \text{RMS(expt)} - \text{RMS(D)}$ (figure 2(*b*)) are clearly associated with the magic neutron numbers $N = 8$, 14, 28, 50, 82 and 126 in that the value of ΔR is small for these values of N. It is notable that there is a minimum at $N = 14$ (the $0d_{5/2}$ shell closure) rather than $N = 20$ ($0d_{3/2}$ shell closure). Small values of ΔR can also be associated with the $Z = 50$ and $Z = 82$ shell closures.

3. Single-particle potential models

The usual starting point for microscopic nuclear models is the Hartree–Fock mean-field theory. Each nucleon is assumed to move independently in a single-particle potential field. Ideally one would start with the experimental nucleon–nucleon interaction and calculate the mean-field potential. In practice this method is limited by the need to restrict the number of allowed Slater-determinant configurations (often to one). Then the effects of all the remaining configurations must be calculated in perturbation theory. Because of the

problems associated with the convergence of this perturbation expansion, calculations starting from the experimental nucleon–nucleon interaction are not very successful. The most successful mean-field calculations have used phenomenological two-body interactions instead. At a less fundamental level, one can also consider some phenomenological form for the mean-field potential itself. In each case a certain limited set of parameters is adjusted to reproduce chosen data. These parameters are usually taken as constants or are assumed to have a smoothly varying dependence on N and Z.

For a spherical potential the total radial density for the point nucleons is given by the orbit occupation times the radial density of the single-particle state $|R(r)|^2$. The charge RMS radii are then obtained from these point-proton radii taking account of the corrections for the finite charge distribution of the protons and neutrons and for the relativistic spin–orbit and Darwin–Foldy corrections; for references and details concerning the method of calculation see Malaguti *et al* (1978, 1979a, b, 1982) and Brown *et al* (1979, 1983). For the orbit occupations we use the integer occupations of the extreme single-particle model obtained by filling the single-particle states in the order of the calculated single-particle energies. (For the harmonic-oscillator potential the order was taken to be $0s_{1/2}$, $0p_{3/2}$, $0p_{1/2}$, $0d_{5/2}$, $0d_{3/2}$, $1s_{1/2}$, $0f_{7/2}$, $0f_{5/2}$, $1p_{3/2}$, $1p_{1/2}$, . . . , etc.)

The single-particle radial wavefunctions are calculated in a formulation which allows for non-local potentials generated from the Skyrme-type interactions (Vautherin and Brink 1972) as well as for the usual local potentials. The radial wavefunctions $R(r)$ can be obtained from a set of equations (Dover and van Giai 1972) involving an equivalent local potential $U_L(r)$ and radial wavefunctions $R_L(r)$

$$\{-(\hbar^2 \, d^2/2\mu \, dr^2) + [\hbar^2 l(l+1)/2\mu r^2] + U_L(r, \varepsilon)\}R_L(r) = \varepsilon R_L(r) \tag{13}$$

where

$$R(r) = (m^*(r)/m)^{1/2} R_L(r) \tag{14}$$

and

$$U_L(r, \varepsilon) = (1 - m^*(r)/m)\varepsilon + (m^*(r)/m)U(r). \tag{15}$$

All of the above functions and the single-particle energies ε depend implicitly on the quantum numbers α (= proton/neutron), n, l and j of the single-particle state. The effective mass $m^*(r)$ is given in terms of the nucleon densities and the Skyrme parameters by equation (2.3) of Dover and van Giai (1972) (see also equation (33) of Brown *et al* (1982)).

The potential $U(r)$ is divided in the usual way into central, spin–orbit and Coulomb components:

$$U(r, \alpha) = V(r, \alpha) + V_{so}(r, \alpha)\langle \boldsymbol{l} \cdot \boldsymbol{\sigma} \rangle + V_{\text{Coulomb}}(r, \alpha). \tag{16}$$

Three forms for the central potential $V(r)$ are considered: the harmonic-oscillator form V_{HO}, the Woods–Saxon form V_{WS} and the form V_{SK} obtained with the Skyrme-type interaction:

$$V_{HO}(r, \alpha) = \tfrac{1}{2} m\omega^2 r^2 \tag{17}$$

$$V_{WS}(r, \alpha) = V_\alpha (1 + \exp(r - R_\alpha)/a_\alpha)^{-1} \tag{18}$$

and

$$V_{SK}(r, \alpha) = F[\alpha, \rho_p(r), \rho_n(r)]. \tag{19}$$

The constants V_α, R_α and a_α are the values of the well depth, radius and diffuseness, respectively, for the Woods–Saxon potential. The Skyrme function F of the proton and neutron densities ρ_p and ρ_n is given by equation (2.12) of Dover and van Giai (1972) (the quantity inside the first square bracket). (Note that in equation (2.5) of Dover and van Giai the term $\frac{1}{2}(t_1 + t_2)$ should be replaced by $\frac{1}{4}(t_1 + t_2)$.)

For the harmonic-oscillator potential, $\hbar\omega$ was assumed to depend smoothly on mass in the form given by Blomqvist and Molinari (1968):

$$\hbar\omega = 45A^{-1/3} - 25A^{-2/3}. \tag{20}$$

The harmonic-oscillator potential is assumed to be local (i.e., $m^*(r)/m = 1$ in the equations above), and the spin–orbit and Coulomb potentials are not included.

The Woods–Saxon potential has six parameters: V_p, R_p, a_p, V_n, R_n and a_n. (The results presented here are insensitive to the neutron potential.) For the selected nuclei ^{16}O, ^{40}Ca and ^{208}Pb, the three proton potential parameters have been uniquely adjusted to reproduce the $\langle r^2 \rangle$ and $\langle r^4 \rangle$ moments of the measured charge distribution and the empirical binding energy of the least bound filled proton orbit (Streets *et al* 1982, Brown *et al* 1982). For other nuclei with $A > 40$ the potential parameters were obtained from a smooth interpolation based on the formula

$$X_\alpha(N, Z) = X_0 \pm X_1(N-Z)/A + X_2 A^{1/3} \tag{21}$$

where the plus sign is for proton and the minus sign is for neutron. X_0, X_1 and X_2 are constants which are obtained from three sets of parameters: the proton parameters for ^{40}Ca and the proton and neutron parameters for ^{208}Pb (Streets *et al* 1982). For $A = 16$–40 the interpolation was based on equation (21) with the same value of X_1 used for $A > 40$ and with X_0 and X_2 determined from the proton parameters for ^{16}O and ^{40}Ca (Brown *et al* 1982). The Woods–Saxon potential is assumed to be local (i.e., $m^*(r)/m = 1$ in the equations above).

For the Woods–Saxon calculations standard forms are used for the Coulomb and spin–orbit terms in equation (16). We use a Coulomb potential based on a uniform charge-density distribution which has total charge number $Z - 1$ and the experimental RMS charge radius. The spin–orbit potential is based on the usual derivative of a Fermi shape and has strength $(\hbar/m_\pi c)^2 V_{so} = 12$ MeV, radius $1.1A^{1/3}$ fm and diffuseness 0.65 fm. The reduced mass is given by $\mu_\alpha = m_\alpha(A-1)/A$.

The Hartree–Fock calculations presented here were obtained with the Skyrme-3 (SK3) interaction of Beiner *et al* (1975) and with the SGII interaction of van Giai and Sagawa (1981a, b). Both the SK3 and SGII interactions give reasonable ground-state properties. However, by introducing a lower power of the density dependence and a modification of the velocity-dependent spin-exchange term, the SGII interaction is improved over SK3 in several respects. It gives a lower compression modulus ($K = 215$), in better agreement with the empirical value deduced from the energy of the giant monopole state, and also gives realistic properties for the other giant resonances including the spin–isospin modes. In addition, the SGII interaction has an attractive pairing matrix element for the particle–particle interaction (van Giai and Sagawa 1981a, b). The Coulomb and spin–orbit potentials were treated in the same way as in the previous Skyrme Hartree–Fock calculations. The Coulomb potential was calculated by folding the Coulomb interaction with the calculated charge density and then adding on the approximation for the exchange term given by Beiner *et al* (1975). We use the spin–orbit potential given by the first term on the right-hand side of equation (2.6) of Dover and van Giai (1972). By convention, the

reduced mass includes a centre-of-mass correction for the total energy (Vautherin and Brink 1972), $\mu_\alpha = m_\alpha A/(A-1)$.

4. Comparison between experiment and theory

The differences RMS(expt) − RMS(theory) with the theoretical radii calculated with the harmonic-oscillator (HO), Woods–Saxon (WS) and Skyrme Hartree-Fock (SK3 and SGII) models are shown in figures 2(*c*)–(*f*). In order to evaluate the comparisons, we distinguish between two kinds of deviations from zero: (1) the average deviation as a smooth function of mass and (2) the local variations from this average. In general it is probably possible to 'fine tune' the potential parameters (which are assumed to be constants or smoothly varying functions of mass) in order to improve the agreement for the average deviation. On the other hand, the local variations are due to more fundamental inadequacies of the models.

Our calculations are strictly applicable only to the closed-shell configurations. Thus we may expect the difference between experiment and theory to be closest to zero for those nuclei which are expected in the extreme single-particle shell model to have closed-shell configurations for protons and/or neutrons. This expectation is born out most clearly with the SGII Hartree–Fock calculation shown in figure 2(*f*). In this case the deviation between experiment and theory is smallest for those nuclei which have neutron numbers 28, 50, 82 and 126, the well known magic numbers for the closed-shell configurations in nuclei. (These systematics suggest that the arbitrary absolute RMS radii chosen for the Dy ($Z=68$) and Er ($Z=70$) isotopes, whose differences are plotted in figure 2 by squares connected by a line, should be reduced by about 0.04 fm.) In addition, the deviation is small for the Sn ($Z=50$) and Pb ($Z=82$) isotopes. The experimental RMS radii for the non-closed-shell nuclei are systematically larger than the SGII calculation.

The comparison with the SK3 calculation in figure 2(*e*) shows a pattern which is very similar to the SGII calculation (figure 2(*f*)) except that the average deviation for the closed-shell nuclei becomes increasingly larger with increasing mass. This difference may be simply due to the fact that the parameters of the SGII interaction were adjusted more accurately than those of the SK3 interaction to fit the RMS radius of ^{208}Pb, and thus we cannot necessarily conclude from this comparison alone that the functional form of the SGII interaction is superior to that of the SK3 interaction.

Relative to these Hartree–Fock calculations the harmonic-oscillator (figure 2(*c*)) and Woods–Saxon (figure 2(*d*)) calculations are not as successful. Although the harmonic oscillator has historically provided a simple approximation with which to calculate nuclear properties, it is not as realistic as the other models we consider and will not be discussed further. The problem with the Woods–Saxon potential is connected with the fact that the calculated average isotope shift (figure 3(*c*)) is too small, especially for light nuclei. The shape and strength of the isovector potential is important in determining the isotope shift. The isovector shape and well depth of our Woods–Saxon potential are assumed, as usual, to vary as $(N-Z)/A$ (equation (21)) and the parameters have been determined by fits to the neutron and proton single-particle levels and density distributions (see § 3). Our comparisons suggest that the simple $(N-Z)/A$ dependence is not adequate. It would be worthwhile to investigate other forms.

The droplet model (figure 2(*b*)) and SGII model (figure 2(*f*)) comparisons are qualitatively similar. However, they differ in detail, for example, in the region between $N=88$ and $N=104$ where the difference between experiment and theory increases for the

droplet model but decreases for the SGII model. The reason for this difference can be seen in the isotope shifts plotted in figure 3(*f*). Relative to the droplet model the SGII model has on average a larger isotope shift just after a closed shell (such as $N=82$). This shell dependence can be associated with the 'pulling out' of the core protons by the valence neutrons. Just after a closed shell the RMS radii of the valence neutron orbits are larger than the average RMS radii of the filled proton and neutron orbits. Due to the strong attractive proton–neutron interaction, the binding energy is maximised when the neutrons and protons overlap as much as possible. This overlap can be increased by 'pulling out' the core protons and/or 'pulling in' the valence neutrons, and the latter is limited to some extent by the density saturation requirements. This shell-dependent 'monopole polarisation' comes out of the Hartree–Fock calculation because of the self-consistency between the density and the potential, but of course does not appear in the non-self-consistent harmonic-oscillator and Woods–Saxon calculations (see figures 3(*b*) and (*c*)).

The monopole polarisation actually accounts for only a small part of the experimental isotope shift anomalies. In order to understand the remaining discrepancies, we need to investigate the role of the higher-multipole ground-state correlations. For nuclei, the quadrupole correlations, which are manifested in the form of vibrational and/or rotational collective motion, are most important. In the vibrating and deformed liquid-droplet models it is well known that the increase in the RMS radius is proportional to the $B(\mathrm{E2})$ value for the electromagnetic excitation of the collective 2^+ state (Uher and Sorensen 1966, Bohr and Mottelson 1969). In the uniform-density sharp-surface approximation, the increase in the RMS radius up to order β^2 in the deformation parameter is given by

$$\Delta\mathrm{RMS}=(2\pi/5)B(\mathrm{E2})/Z^2\mathrm{RMS}_0^3. \tag{22}$$

(The effect of including terms up to order β^3 (Dobaczewski *et al* 1984) is small (about a -10% correction to $\Delta\mathrm{RMS}$ for $\beta=0.6$) and will be ignored here.)

The quantities $\Delta\mathrm{RMS}$ are plotted in figure 4. They were obtained from equation (22) for the even–even nuclei using experimental $B(\mathrm{E2}, 0^+\rightarrow 2^+)$ values for the lowest 2^+ states and the extended-liquid-drop model (equation (2)) for the zeroth-order radii RMS_0. (The particular Z value of each chain in figure 4 can be inferred from the labels at the top of the figures which are placed directly above the data.) The experimental $B(\mathrm{E2})$ values were taken from the standard compilations: the individual references given on page ii of *Nuclear Data Sheets* (1982) (for lifetimes and excitation energies) and Stelson and Grodzins (1966) (for internal conversion coefficients) for $A>44$, Endt and van der Leun (1978) for $A=21$–44 and Ajzenberg-Selove (1983) for $A=18$–20. Unfortunately, some of the compilations for $A>44$ are somewhat out of date and experimental $B(\mathrm{E2})$ values are not known for all of the nuclei of interest. Nevertheless, comparison of figures 2(*f*) and 4 shows that equation (22) evaluated for the lowest 2^+ states can account qualitatively for the deviation between the experimental RMS radii and those calculated in the spherical SGII Hartree–Fock model. A more quantitative comparison of this kind requires a more up-to-date evaluation of the $B(\mathrm{E2})$ data for $A>44$.

Equation (22) can be extended to states with non-zero spin J_i by replacing $B(\mathrm{E2}, 0^+\rightarrow 2^+)$ with a sum over all possible final states J_f and adding the diagonal quadrupole moment term Q for $J_\mathrm{i}>\frac{1}{2}$ (Brown 1984):

$$B(\mathrm{E2})=\sum B(\mathrm{E2}, J_\mathrm{i}\rightarrow J_\mathrm{f})+(5/16\pi)\{(J_\mathrm{i}+1)(2J_\mathrm{i}+3)/[J_\mathrm{i}(2J_\mathrm{i}-1)]\}Q^2. \tag{23}$$

It would be interesting to see if the odd–even staggering in the RMS radii is correlated with experimental $B(\mathrm{E2})$ values. However, the $B(\mathrm{E2})$ data needed for the odd–even nuclei are

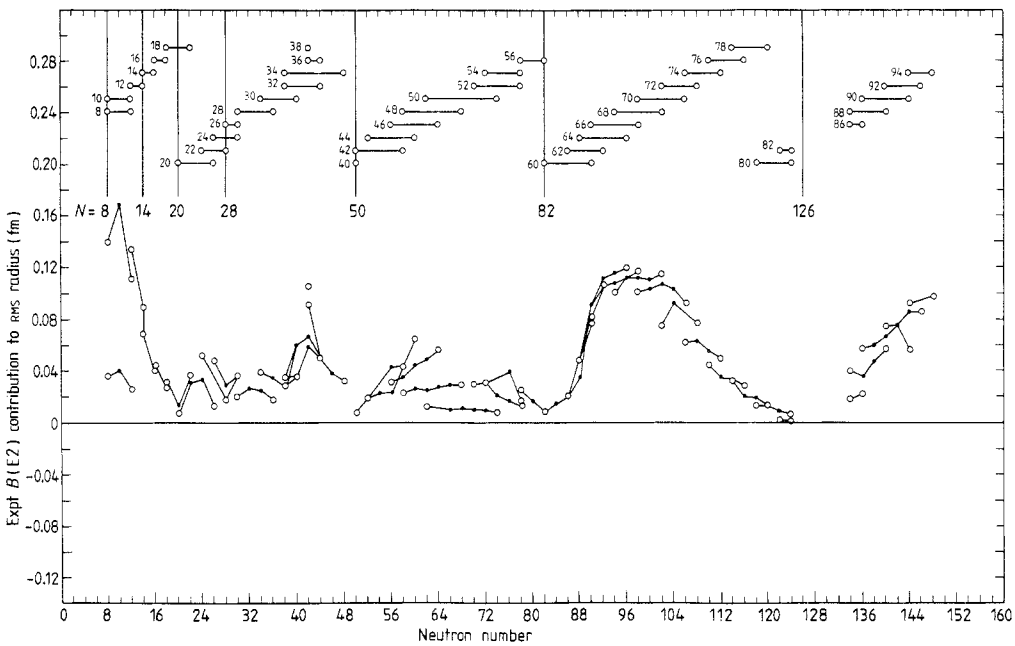

Figure 4. The change in RMS radius based on equation (22) using experimental B(E2) values.

harder to obtain experimentally, and a critical evaluation and summary of the available data are needed.

Esbensen and Bertsch (1983) have recently investigated the ground-state correlation effects associated with the higher multipole vibrational states and the 'giant resonances'. They calculated the change of the mean-square radius in the uniform-density sharp-surface approximation in terms of the mean-square fluctuation of the nuclear radius σ and obtained

$$\langle r^2\rangle - \langle r^2\rangle_{\mathrm{HF}} = 3(\sigma^2_{\mathrm{RPA}} - \sigma^2_{\mathrm{HF}}) \tag{24}$$

where

$$\sigma^2 = (R_0^2/4\pi)\sum \beta_\lambda^2$$

and

$$\beta_\lambda^2 = B(\mathrm{E}\lambda, 0^+ \rightarrow \lambda)[(3/4\pi)ZR_0^\lambda]^{-2}$$

and R_0 is the sharp-surface radius ($R_0^2 = \frac{5}{3}\langle r^2\rangle_{\mathrm{HF}}$). The sum extends over all excited states. The quantity σ_{HF} is the mean-square fluctuation already present in the uncorrelated Hartree–Fock ground state and σ_{RPA} is the mean-square fluctuation due to the correlated states which can be calculated, for example, by the method of the random-phase approximation (RPA). Equation (24) is equivalent to equation (22) when a single $\lambda = 2$ state is considered and $\sigma_{\mathrm{RPA}} \gg \sigma_{\mathrm{HF}}$.

It is useful to distinguish three regions of excitation energy for the collective excitations: (1) the 'high-energy' giant resonance vibrations starting at about $58A^{-1/3}$ in excitation energy, (2) the 'medium-energy' vibrations with $\lambda = 2$–5 around $15A^{-1/3}$ in excitation energy and (3) the 'low-energy' quadrupole vibrations and rotations below 2 MeV in excitation energy. Esbensen and Bertsch found that the contribution of the 'high-energy' giant resonance states in equation (24) was small due to a cancellation between

σ_{RPA} and σ_{HF}. They found that the largest contributions to equation (24) for ^{40}Ca and ^{208}Pb were from the 'medium-energy' states, and in particular from the lowest octupole state.

The total increases in the RMS radii obtained by Esbensen and Bertsch were $\Delta_{RMS} \approx 0.13$ fm for ^{40}Ca and $\Delta_{RMS} \approx 0.020$ fm for ^{208}Pb. Relative to the scale of figure 2, this increase for ^{40}Ca is large and would make the deviation from zero much worse for all of the calculations. However, this is not surprising since the potential parameters have already been adjusted to fit the properties of these nuclei. Rather, what is most important for our comparisons is the detailed mass dependence of the B(E3) for the low-lying octupole vibrations. Unfortunately, systematic experimental information on this is difficult to obtain away from the 'closed-shell' nuclei because the octupole states become fragmented and embedded in a region of relatively high level density. We have not attempted to evaluate the data available. For the purpose of the present discussions, we have assumed that the contributions of these 'medium-energy' excitations to the RMS radii are smoothly mass dependent and have already been incorporated into the potential parameters.

Finally, we discuss the sharp discontinuities which appear in the experimental isotope shifts (figure 3(*a*)). These are usually attributed to a sudden transition from a spherical ground-state to a deformed ground-state configuration. The sharp discontinuities in the calculated isotope shifts (figures 3(*c*)–(*f*)) occur for a different reason. These appear when the highest j orbit from the unfilled shell passes through the orbits of the valence shell. This causes an irregular isotope shift directly in the case of protons due to the difference in the RMS radius of the orbits in the two major shells and indirectly in the case of neutrons due to the contribution from the neutron spin–orbit charge distribution. In the Hartree–Fock calculations the crossing of neutron orbits also contributes indirectly due to their influence on the proton potential. (For the SK3 calculations the isotope shifts are also shown without the addition of the neutron finite-size and neutron spin–orbit contributions (SK3b) in figure 3(*e*) in order to show their relative contribution to the isotope shifts.) The sharp discontinuities in the experimental isotope shift (figure 3(*a*)) do not occur in the same place as those calculated. However, this aspect of the calculation is particularly sensitive to the orbit occupations. We have assumed integer orbit occupations determined by the ordering of the levels in the spherical potentials (see § 3). Configuration mixing in the open-shell nuclei will smooth out the orbit occupations and wash out the sharp structures in the calculation. In future studies it would be interesting to consider the effects of level crossing in a deformed potential.

Acknowledgments

We would like to thank Mr R J M Sweet for help in compiling the information on B(E2) values. This research was supported in part by National Science Foundation Grants Nos PHY-80-17605 and PHY-83-12245.

References

Ajzenberg-Selove F 1983 *Nucl. Phys.* A **392** 1

Andl A, Bekk K, Göring S, Hanser A, Nowicki G, Rebel H, Schatz G and Thompson R C 1982 *Institut für Angewandte Kernphysik, KfK Karlsruhe, Preprint*

Barrett R C and Jackson D F 1977 *Nuclear Sizes and Structure* (Oxford: Clarendon)

Beiner M, Flocard H, van Giai N and Quentin P 1975 *Nucl. Phys.* A **238** 29
Bekk K, Andl A, Göring S, Hanser A, Nowicki G, Rebel H and Schatz G 1979 *Z. Phys.* A **291** 219
Blomqvist J and Molinari A 1968 *Nucl. Phys.* A **106** 545
Boehm F and Lee P L 1974 *Atomic and Nuclear Data Tables* **14** 605
Bohr A and Mottelson B R 1969 *Nuclear Structure* vol. I (New York: Benjamin)
Bonn J, Huber G, Kluge H-J and Otten E W 1976 *Z. Phys.* A **276** 203
Briscoe W J, Crannell H and Bergstrom J C 1980 *Nucl. Phys.* A **344** 475
Brix P and Kopfermann H 1958 *Rev. Mod. Phys.* **30** 517
Brown B A 1984 unpublished
Brown B A, Massen S E, Escudero J I, Hodgson P E, Madurga G and Vinas J 1983 *J. Phys. G: Nucl. Phys.* **9** 423
Brown B A, Massen S E and Hodgson P E 1979 *J. Phys. G: Nucl. Phys.* **5** 1655
Brown B A, Wildenthal B H, Chung W, Massen S E, Bernas M, Bernstein A M, Miskimen R, Brown V R and Madsen V A 1982 *Phys. Rev.* C **26** 2247
Bumiller F A, Buskirk F R, Dyer J N and Monson W A 1972 *Phys. Rev.* C **5** 391
Cavedon J M 1980 *PhD Thesis* Orsay
Chandra H and Sauer G 1976 *Phys. Rev.* C **13** 245
Daniel H, Pfeiffer H-J, Springer K, Stoeckel P, Backenstoss G and Tauscher L 1974 *Phys. Lett.* **48B** 109
Dobaczewski J, Vogel P and Winter A 1984 *Phys. Rev.* C **29** 1540
Dover C B and van Giai N 1972 *Nucl. Phys.* A **190** 373
van Eijk C W, Wijnhorst J, Popelier M A and Gillespie W A 1979 *J. Phys. G: Nucl. Phys.* **5** 315
Endt P M and van der Leun C 1978 *Nucl. Phys.* A **310** 1
Engfer R, Schneuwly H, Vuilleumier J L, Walter H K and Zehnder A 1974 *Atomic and Nuclear Data Tables* **14** 509
Esbensen H and Bertsch G F 1983 *Phys. Rev.* C **28** 355
Euteneuer H *et al* 1977 *Phys. Rev.* C **16** 1703
Finn J M, Crannell H, Hallowell P L, O'Brien J T and Penner S 1976 *Nucl. Phys.* A **274** 28
Fricke G *et al* 1982 *SIN Newsletter* no 14 61
Gerhardt H, Matthias E, Rinneberg H, Schneiderm F, Timmermann A, Wenz R and West P J 1979 *Z. Phys.* A **292** 7
van Giai N and Sagawa H 1981a *Nucl. Phys.* A **371** 1
—— 1981b *Phys. Lett.* **106B** 379
Gillespie W A, Brain S W, Johnston A, Lees E W, Singhal R P, Slight A G, Brimicombe M W S, Stacey D N, Stacey V and Huhnermann H 1975 *J. Phys. G: Nucl. Phys.* **1** L6
Heilig K and Steudel A 1974 *Atomic and Nuclear Data Tables* **14** 613
Huber G *et al* 1978 *Phys. Rev.* C **18** 2342
de Jager C W, de Vries H and de Vries C 1974 *Atomic and Nuclear Data Tables* **14** 479
Kim J C, Hicks R S, Yen R, Auer I P, Caplan H S and Bergstrom J C 1978 *Nucl. Phys.* A **297** 301
Kline F J, Auer I P, Bergstrom J C and Caplan H S 1975 *Nucl. Phys.* A **255** 435
Kluge H-J, Kremmling H, Schuessler H A, Streib J and Wallmeroth K 1983 *Z. Phys.* A **309** 187
Laubacher D B, Tanaka Y, Steffen R M, Shera E B and Hoehn M Y 1983 *Phys. Rev.* C **27** 1772
Li C G, Yearian M R and Sick I 1974 *Phys. Rev.* C **9** 1861 and private communication
Lightbody J W, Penner S, Fivozinsky S P, Hallowell P L and Crannell H 1976 *Phys. Rev.* C **14** 952
Lightbody J W *et al* 1983 *Phys. Rev.* C **27** 113
McCarthy J S, Sick I and Whitney R R 1977 *Phys. Rev.* C **15** 1396
Malaguti F, Uguzzoni A, Verondini E and Hodgson P E 1978 *Nucl. Phys.* A **297** 206
—— 1979a *Nuovo Cimento* A **49** 412
—— 1979b *Nuovo Cimento* A **53** 1
—— 1982 *Riv. Nuovo Cimento* **5** 1
Miska H, Norum B, Hynes M V, Bertozzi W, Kowalski S, Rad F N, Sargent C P, Sasanuma T and Berman B L 1979 *Phys. Lett.* **83B** 165
Moinester M A, Alster J, Azuelos G, Bellicard J B, Frois B, Huet M, Leconte P and Ho P X 1981 *Phys. Rev.* C **24** 80
Myers W D 1977 *Droplet Model of the Nucleus* (New York: IFI/Plenum Data Co.)
—— 1982 *Proc. Conf. on Lasers in Nuclear Physics* ed. C E Bemis and H K Carter (New York: Harwood Academic) p 437 and references therein
Myers W A and Schmidt K H 1983 *Nucl. Phys.* A **410** 61
Neugart R 1982 *Proc. Conf. on Lasers in Nuclear Physics* ed. C E Bemis and H K Carter (New York: Harwood Academic) p 231 and references therein

Nuclear Data Sheets 1982 vol. 36 no 2
Olin A, Poffenberger R R, Beer G A, Macdonald J A, Mason G R, Pearce R M and Sperry W C 1981 *Nucl. Phys.* A **360** 426
Reehal B S and Sorensen R A 1971 *Nucl. Phys.* A **161** 385
Rothhaas H 1976 *PhD Thesis* Universität Mainz
Rychel D, Emrich H J, Miska H, Gyufko R and Weidner C A 1983 *Phys. Lett.* **130B** 5
Schaller L A, Dubler T, Kaeser K, Rinker G A, Robert-Tissot B, Schellenberg L and Schneuwly H 1978 *Nucl. Phys.* A **300** 225
Schaller L A, Schellenberg L, Phanm, T Q, Piller G, Reutschi A and Schneuwly H 1982 *Nucl. Phys.* A **379** 523
Schellenberg L, Robert-Tissot B, Kaeser K, Schaller L A, Schneuwly H, Fricke G, Gluckert S, Mallot G and Shera E B 1980 *Nucl. Phys.* A **333** 333
Schinzler B, Klempt W, Kaufman S L, Lochmann H, Moruzzi G, Neugart R, Otten E-W, Bonn J, Von Reisky L, Spath K P C, Steinacher J and Westkott D 1978 *Phys. Lett.* **79B** 209
Schütz W 1975 *Z. Phys.* A **273** 69
Shera E B, Ritter E T, Perkins R B, Rinker G A, Wagner L K, Wohlfahrt H D, Fricke G and Steffen R M 1976 *Phys. Rev.* C **14** 731
Shera E B, Wohlfahrt H D, Hoehn M V and Tanaka Y 1982 *Phys. Lett.* **112B** 124
Sick I, McCarthy J S and Whitney R R 1976 *Phys. Lett.* **64B** 33
Singhal R P, Caplan H S, Moreira J R and Drake T E 1975 *Can. J. Phys.* **51** 2125
Sorensen R A 1966 *Phys. Lett.* **21** 333
Stelson P H and Grodzins L 1966 *Nuclear Data Tables* **1** 21
Streets J, Brown B A and Hodgson P E 1982 *J. Phys. G: Nucl. Phys.* **8** 839
Suelzle L R, Yearian M R and Crannell H 1967 *Phys. Rev.* **162** 992
Thibault C *et al* 1981a *Phys. Rev.* C **23** 2720
—— 1981b *Nucl. Phys.* A **367** 1
Thompson R C, Anselment M, Bekk K, Goring S, Hanser A, Meisel G, Rebel H, Schatz G and Brown B A 1983 *J. Phys. G: Nucl. Phys.* **9** 443
Touchard F *et al* 1982 *Phys. Lett.* **108B** 169
Uher R A and Sorensen R A 1966 *Nucl. Phys.* **86** 1
Vautherin D and Brink D M 1972 *Phys. Rev.* C **5** 626
Wenz R, Timmermann A and Matthias E 1981 *Z. Phys.* A **303** 87
Wohlfahrt H D, Schwentker O, Fricke G, Anderson H G and Shera E B 1980 *Phys. Rev.* C **22** 264
Wohlfahrt H D, Shera E B, Hoehn M V, Yamazaki Y and Steffen R M 1981 *Phys. Rev.* C **23** 533